AT&T Technical Journal
Vol. 64, No. 6, July–August 1985
Printed in U.S.A.

Digital Transmission Over Cross-Coupled Linear Channels

By J. SALZ*

(Manuscript received January 14, 1985)

For a multiuser data communications system operating over a mutually cross-coupled linear channel with additive noise sources, we determine the following: (1) a linear cross-coupled receiver processor (filter) that yields the least-mean-squared error between the desired outputs and the actual outputs, and (2) a cross-coupled transmitting filter that optimally distributes the total available power among the different users, as well as the total available frequency spectrum. The structure of the optimizing filters is similar to the known 2 x 2 case encountered in problems associated with digital transmission over dually polarized radio channels.

I. INTRODUCTION

A variety of communication channels can be modeled as multi-input, multi-output, mutually cross-coupled linear networks with additive noise sources. A few examples of communications systems operating over such channels are dually polarized radio systems, frequency/time-division multiplexing with crosstalk, cordless PBXs, spread-spectrum multiuser systems, and multisensor radar/sonar systems. In many applications it is beneficial to design cross-coupled transmitters and receivers that take advantage of the inherent mutual interferences. The chief purpose of this paper is to explore these issues from a theoretical point of view.

The general problem we address follows. We consider an N input-

* AT&T Bell Laboratories.

port, N output-port, linear transmission channel characterized by an N x N complex matrix frequency transfer function, $\mathbf{C}(\omega)$, where the entries in $\mathbf{C}(\omega)$, $C_{ij}(\omega)$, $i, j = 1 \ldots N$, represent the transfer characteristics from input i to output j. Digital data signals $D_i(t)$, $i = 1 \cdots N$ are intended for simultaneous transmission over this medium. The general problem we address is as follows: how does one jointly optimize the $2N^2$ entries of cross-coupled linear receiving and transmitting matrix filters when the performance criterion is total Mean-Squared Error (MSE) subject to a constraint on the total average transmitted power? The general setup is shown schematically in Fig. 1.

This paper includes generalizations to $N(N \geq 2)$ dimensions of earlier work dealing with digital data transmission over dually polarized radio channels.[1,2] As far as can be determined, these generalizations have not been reported in the open literature. We found, however, two early papers[3,4] dealing with multi-input, multi-output, communications that might be of interest to the reader in connection with our problem. For additive Gaussian noise sources the Shannon capacity of the type of channel considered here has also been determined.[5]

After formulating the problem in the next section, we derive the optimal matrix receiving filter structure and provide a closed-form formula for the least MSE. In Section IV we address and solve the optimum transmitter problem, while the last section has our concluding remarks.

II. PROBLEM FORMULATION

Consider a linear communications medium characterized by N^2 (N is an arbitrary integer) real impulse response functions,

$$h_{lj}(t) = \int_{-\infty}^{\infty} H_{lj}(\omega) e^{i\omega t} \frac{d\omega}{2\pi}, \qquad l, j = 1, 2 \cdots N, \tag{1}$$

where $H_{lj}(\omega)$, $l, j = 1 \cdots N$ are the complex frequency transfer characteristics from input l to output j. The representation in (1) characterizes a linear medium with N inputs and N outputs where

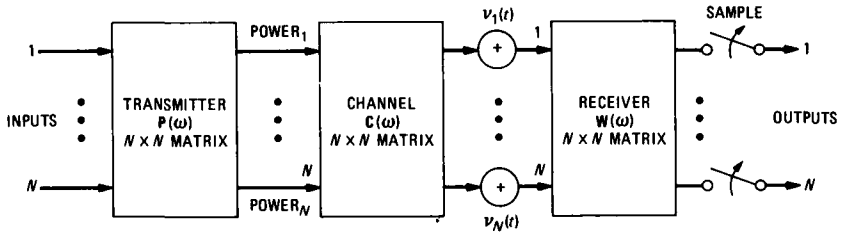

Fig. 1—Multi-input, multi-output data communications.

$h_{ij}(t)$ is interpreted as the output of the jth medium when the lth input is a unit impulse. More compactly, let $\mathbf{h}(t)$ represent the N x N impulse response matrix with entries $h_{ij}(t)$. Now the diagonal entries stand for the direct-channel impulse responses, while the off-diagonal terms are the cross-interference impulse responses.

In the present situation we have in mind that N real data signals,

$$D_l(t) = \sum_n a_n^{(l)} g(t - nT), \qquad l = 1 \cdots N, \tag{2}$$

where $\{a_n^{(l)}\}$ are the data symbols, are intended for simultaneous transmission over the N channels. Mutual dispersive cross coupling, intersymbol interference, and noise distort these signals, and the purpose here is to devise transmitting and receiving processors to mitigate against these interferences.

The present model also accommodates bandpass coherent data signals in which case (2) represents the baseband-equivalent signals with complex data symbols. In our general formulation, however, we can get by with only real data symbols since complex numbers are isomorphic to 2 x 2 real matrices.*

Returning to the general formulation, the N data sequences are now represented by the column vectors

$$\mathbf{A}_n = \begin{bmatrix} a_n^{(1)} \\ \vdots \\ a_n^{(N)} \end{bmatrix}, \text{ all } n,$$

and the data signal is thus represented by an N-dimensional vector,

$$\mathbf{D}(t) = \sum_n \mathbf{A}_n g(t - nT). \tag{3}$$

Consequently, the channel output signal can be represented as the vector time function,

$$\mathbf{S}(t) = \sum_n \mathbf{H}(t - nT)\mathbf{A}_n, \tag{4}$$

where the matrix $\mathbf{H}(t)$ is the convolution

$$\mathbf{H}(t) = \int_{-\infty}^{\infty} g(t - \tau)\mathbf{h}(\tau)\mathbf{d}\tau, \tag{5}$$

and the N x N matrix $\mathbf{h}(t)$ has entries defined in (1).

For the sake of clarity, we restrict our treatment to N x N transmitter and receiver filters, while we recognize applications where it

* References 1 and 2 exploit this isomorphism effectively in the treatment of quadrature amplitude modulated systems over bandpass channels.

would be necessary to handle nonsquare matrices. This does not, however, restrict our approach, as will become evident.

Proceeding with the analysis, we presume that a noise vector $\nu(t)$ is added to (4) and the sum signal is passed through an N x N matrix receiver filter denoted by $\mathbf{W}(t)$. A representative sample of the output vector taken at $t = 0$ (without loss of generality) yields

$$\mathbf{S}_0 = \mathbf{U}_0\mathbf{A}_0 + \sum_{\substack{n \\ n\neq 0}} \mathbf{U}_n\mathbf{A}_n + \nu_0, \tag{6}$$

where

$$\mathbf{U}_n = \int_{-\infty}^{\infty} \mathbf{W}(-\tau)\mathbf{H}(\tau - nT)\mathbf{d}\tau$$

and

$$\nu_0 = \int_{-\infty}^{\infty} \mathbf{W}(-\tau)\nu(\tau)\mathbf{d}\tau.$$

We now regard the vector $\tilde{\mathbf{S}}_0$ [a suitably quantized version of $\mathbf{S}_0$ in (6)] as an estimate of the data vector $\mathbf{A}_0$. Thus the system designer has the freedom to choose the receiver matrix $\mathbf{W}(t)$ and a transmitting filter (yet unspecified) to make $\tilde{\mathbf{S}}_0$ as close as possible, in some reasonable sense, to the desired quantity. While the most objective sense in which this can be made close to $\mathbf{A}_0$ is

$$\text{probability } [\tilde{\mathbf{S}}_0 \neq \mathbf{A}_0] < \delta$$

for a given δ, it is not a mathematically tractable quantity to work with, and therefore a simpler cost function is sought. As is well known, the probability of error cannot be expressed exactly even when the added noise is assumed to be Gaussian—a difficulty caused by the presence of intersymbol and cross-channel interference. Here we employ a simple cost-function, least-mean-squared error between $\mathbf{S}_0$ and $\mathbf{A}_0$. This criterion, which lends itself to mathematical analysis, can also be used to upper bound the probability of error when the added noise is Gaussian.

Returning to the mathematical problem at hand, we thus define the error vectors ϵ as the difference between $\mathbf{S}_0$, eq. (6), and the desired data vector $\mathbf{A}_0$. The total Mean-Squared Error ($\overline{\text{MSE}}$) then is

$$\overline{\text{MSE}} = \mathbf{E}\{\epsilon^+\epsilon\} = \text{tr}[\mathbf{E}\{\epsilon\epsilon^\dagger\}], \tag{7}$$

where

$$\epsilon = (\mathbf{U}_0 - \mathbf{I})\mathbf{A}_0 + \sum_{\substack{n \\ n\neq 0}} \mathbf{U}_n\mathbf{A}_n + \nu_0. \tag{8}$$

In (7) tr stands for the trace of a matrix, † the complex conjugate transpose, and $E(\cdot)$ the mathematical expectation with respect to all random variables.

Without loss of generality, we assume that the data symbols as well as the vector sequences $\mathbf{A}_n$ are independent and identically distributed, as are the added noise components in $\nu(t)$. With these assumptions the detailed evaluation of (7) becomes

$$\mathrm{MSE} = \frac{\overline{\mathrm{MSE}}}{\sigma_d^2} = \mathrm{tr}\Bigg[\mathbf{I} - 2\int_{-\infty}^{\infty} \mathbf{W}(-\tau)\mathbf{H}(\tau)\mathbf{d}\tau + \sigma^2 \int_{-\infty}^{\infty} \mathbf{W}(-\tau)\mathbf{W}^\dagger(-\tau)\mathbf{d}\tau + \sum_{\substack{n \\ n\neq 0}} \int_{-\infty}^{\infty} \mathbf{W}(-\tau)\mathbf{H}(\tau - nT)\mathbf{d}\tau \int_{-\infty}^{\infty} \mathbf{H}^\dagger(\tau - nT)\mathbf{W}^\dagger(-\tau)\mathbf{d}\tau\Bigg], \quad (9)$$

where

$$E\{\mathbf{A}_n\mathbf{A}_n^\dagger\} = \sigma_d^2\mathbf{I},$$

$$E\{\nu(t)\nu^\dagger(t)\} = N_0\mathbf{I},$$

and

$$\sigma^2 = \frac{N_0}{\sigma_d^2}.$$

Recall that when the data symbols $\{a_n^{(l)}\}$ take on values, $\pm 1 \pm 3 \pm \cdots \pm(L-1)$, $E\{a_n^{(l)}\} = \sigma_d^2 = L^2 - 1/3$.

In the next section (9) is first minimized with respect to the class of all N x N real matrices for a given channel matrix $\mathbf{H}$ and parameter σ^2, and in Section IV it is further minimized with respect to the admissible class of transmitter filters.

III. THE RECEIVER OPTIMIZATION PROBLEM

It turns out that the mathematical machinery used in the selection of the optimum N x N, $\mathbf{W}(t)$, is the same as that for the 4 x 4 case developed in Ref. 2, so here we only briefly review the approach.

Proceeding with the optimization problem, replace $\mathbf{W}(t)$ by

$$(\mathbf{W}_0)_{ij} + (\zeta\eta)_{ij}, \qquad i, j = 1, \cdots, N, \quad (10)$$

where η_{ij} are arbitrary functions of τ, and set

$$\frac{\partial}{\partial \zeta_{ij}} (\mathrm{MSE}) = [\mathbf{0}]_{ij}$$

at $\zeta_{ij} = 0$, $i, j = 1, \cdots, N$.

Now compute

$$\frac{\partial}{\partial \zeta_{ij}} (\text{MSE}) = \text{tr}\left[-2 \int_{-\infty}^{\infty} \eta_{ij}^0(\tau)\mathbf{H}(\tau)\mathbf{d}\tau + 2\sigma^2 \int_{-\infty}^{\infty} \mathbf{W}_0(-\tau)\eta_{ji}^0(\tau)\mathbf{d}\tau \right.$$

$$\left. + 2 \sum_{\substack{n \\ n\neq 0}} \int_{-\infty}^{\infty} \mathbf{W}_0(\tau)\mathbf{H}(\tau - nT)\mathbf{d}\tau \int_{-\infty}^{\infty} \mathbf{H}^\dagger(\tau - nT)\eta_{ji}^0(\tau)\mathbf{d}\tau\right] = 0,$$

$$i, j = 1, \cdots, N, \quad (11)$$

where the matrices, η_{ij}^0, $i, j = 1, \cdots, N$ have the entry $\eta_{ij}(\tau)$ in the ijth position and zero everywhere else. By a direct computation of the trace in eq. (11), one obtains

$$-\int_{-\infty}^{\infty} (\mathbf{H}(\tau))_{ji}\eta_{ij}(\tau)\mathbf{d}\tau + \sigma^2 \int_{-\infty}^{\infty} (\mathbf{W}(-\tau))_{ij}\eta_{ij}(\tau)\mathbf{d}\tau$$

$$+ \sum_{\substack{n \\ n\neq 0}} \int_{-\infty}^{\infty} [\mathbf{H}(\tau - nT)\mathbf{U}_n^\dagger]_{ji}\eta_{ij}(\tau)\mathbf{d}\tau = 0, \qquad i, j = 1, \cdots, N. \quad (12)$$

Since eq. (12) must hold for all functions, $\eta_{ij}(\tau)$, we obtain the matrix integral equation that must be satisfied by the optimum matrix $\mathbf{W}_0(\tau)$,

$$\sigma^2\mathbf{W}_0(-\tau) = \mathbf{H}^\dagger(\tau) - \sum_{\substack{n \\ n\neq 0}} \mathbf{U}_n\mathbf{H}^\dagger(\tau - nT), \quad (13)$$

where $\mathbf{U}_n$ is given in eq. (6) with $\mathbf{W}(\tau)$ replaced by $\mathbf{W}_0(\tau)$. Structurally, $\mathbf{W}_0(\tau)$ consists of an N x N matrix-matched filter followed by a matrix-tapped delay line with matrix-tap coefficients $\mathbf{U}_n$.

An explicit formula for the least MSE is now possible to obtain by first post-multiplying eq. (13) by $\mathbf{W}_0^\dagger(-\tau)$, integrating, and then comparing the result with eq. (9). The result is

$$\text{MSE}_0 = \text{tr}[\mathbf{I} - \mathbf{U}_0], \quad (14)$$

where $\mathbf{U}_0$ is obtained by solving a set of infinite linear equations obtained by first post-multiplying eq. (13) by $\mathbf{H}(\tau - kT)$ and then integrating. These operations yield the equations

$$\sigma^2\mathbf{U}_k = \mathbf{R}_k - \sum_{\substack{n \\ n\neq 0}} \mathbf{U}_n\mathbf{R}_{k-n}, \text{ all } k$$

$$= \mathbf{R}_{-k}^\dagger, \quad (15)$$

where

$$\mathbf{R}_k = \int_{-\infty}^{\infty} \mathbf{H}^\dagger(\tau)\mathbf{H}(\tau - kT)\mathbf{d}\tau. \quad (16)$$

The matrix convolutional equation, (15), is easy to solve by Fourier series methods. Thus, inserting the solution of $\mathbf{U}_0$, obtained from (15), into (14), we get

$$\mathrm{MSE}_0 = \frac{1}{2\pi} \int_{-\pi}^{\pi} \mathrm{tr} \left[\mathbf{I} + \frac{\mathbf{R}(\omega)}{\sigma^2} \right]^{-1} \mathbf{d}\omega, \tag{17}$$

where

$$\mathbf{R}(\omega) = \sum_k \mathbf{R}_k e^{i\omega kT}$$

and

$$\begin{aligned} \mathbf{R}_k &= \frac{T}{2\pi} \int_{-\pi/T}^{\pi/T} \mathbf{R}(\omega) e^{-i\omega kT} \mathbf{d}\omega, \\ &= \int_{-\infty}^{\infty} \mathbf{H}^\dagger(\tau) \mathbf{H}(\tau - kT) \mathbf{d}\tau \end{aligned} \tag{18}$$

[from (16)].

Now the matrix frequency transfer characteristic is, by definition,

$$\tilde{\mathbf{H}}(\omega) = \int_{-\infty}^{\infty} \mathbf{H}(t) e^{i\omega t} \mathbf{d}t,$$

and, by Parseval's theorem, (18) is put into the form

$$\begin{aligned} \mathbf{R}_k &= \frac{1}{2\pi} \int_{-\infty}^{\infty} \tilde{\mathbf{H}}^\dagger(\omega) \tilde{\mathbf{H}}(\omega) e^{-i\omega kT} \mathbf{d}\omega \\ &= \frac{1}{2\pi} \int_{-\pi/T}^{\pi/T} \sum_k \tilde{\mathbf{H}}^\dagger \left(\omega - \frac{2\pi k}{T} \right) \tilde{\mathbf{H}} \left(\omega - \frac{2\pi k}{T} \right) e^{-i\omega kT} \mathbf{d}\omega. \end{aligned} \tag{19}$$

From this and (18) we determine

$$\mathbf{R}(\omega) = \frac{1}{T} \sum_k \tilde{\mathbf{H}}^\dagger \left(\omega - \frac{2\pi k}{T} \right) \tilde{\mathbf{H}} \left(\omega - \frac{2\pi k}{T} \right), \tag{20}$$

which is the matrix-folded, or aliased, channel spectrum.

In the next section we further minimize MSE, eq. (17), with respect to the transmitter matrix filter.

IV. TRANSMITTER OPTIMIZATION

The general optimization problem with the inclusion of the aliases, eq. (20), appears to be extremely complicated to solve,* and therefore

* We refer the interested reader to Ref. 6, where a similar optimization problem is solved without having to make the bandlimited assumption.

we shall assume that the transmitter filter is strictly bandlimited to the Nyquist frequency, π/T. So, without excess bandwidth, (20) reduces to

$$\mathbf{R}(\omega) = \frac{1}{T}\,\tilde{\mathbf{H}}^{\dagger}(\omega)\tilde{\mathbf{H}}(\omega), \tag{21}$$

and since the transmitter matrix filter is in cascade with the channel filter, we can write

$$\tilde{\mathbf{H}}(\omega) = \mathbf{C}(\omega)\mathbf{P}(\omega). \tag{22}$$

Equation (2) now becomes

$$\mathbf{R}(\omega) = \frac{1}{T}\,\mathbf{P}^{\dagger}(\omega)\mathbf{C}^{\dagger}(\omega)\mathbf{C}(\omega)\mathbf{P}(\omega), \tag{23}$$

where $\mathbf{C}(\omega)$ is the transmission medium frequency transfer characteristic and $\mathbf{P}(\omega)$ represents the N x N matrix transmitting filter frequency characteristics.

Note that the average total transmitted power is proportional to

$$\int_{-\pi/T}^{\pi/T} \mathrm{tr}[\mathbf{P}^{\dagger}(\omega)\mathbf{P}(\omega)]\mathbf{d}\omega,$$

and therefore the quantity we wish to minimize with respect to $\mathbf{P}(\omega)$ is, from (17) and (23),

$$F = \int_{-\pi/T}^{\pi/T} \mathrm{tr}\left[\mathbf{I} + \frac{1}{\sigma^2 T}\,\mathbf{P}^{\dagger}(\omega)\mathbf{C}^{\dagger}(\omega)\mathbf{C}(\omega)\mathbf{P}(\omega)\right]^{-1}\mathbf{d}\omega + \lambda \int_{-\pi/T}^{\pi/T} \mathrm{tr}[\mathbf{P}^{\dagger}(\omega)\mathbf{P}(\omega)]\mathbf{d}\omega, \tag{24}$$

where λ is a Lagrange multiplier to be determined from the power constraint.

Since for each value of ω, $\mathbf{C}^{\dagger}\mathbf{C}$ is hermitian, nonnegative definite, it can be diagonalized by a unitary matrix ψ,

$$\mathbf{C}^{\dagger}(\omega)\mathbf{C}(\omega) = \psi^{\dagger}(\omega)\mathbf{\Lambda}(\omega)\psi(\omega), \tag{25}$$

where $\mathbf{\Lambda}(\omega)$ is the diagonal matrix with entries, $\lambda_1 \cdots \lambda_N$, the eigenvalues of $\mathbf{C}^{\dagger}\mathbf{C}$. By letting $\mathbf{G} = \psi\mathbf{P}$, $\mathbf{Q} = \mathbf{G}\mathbf{G}^{\dagger}$, and scaling the eigenvalues by $1/\sigma^2 T$, (24) is put into the form

$$F = \int_{-\pi/T}^{\pi/T} \mathrm{tr}\{(\mathbf{I} + \mathbf{Q}\mathbf{\Lambda})^{-1} + \lambda\mathbf{Q}\}\mathbf{d}\omega, \tag{26}$$

where we have used an innocuous result,

$$\mathrm{tr}[\mathbf{I} + \mathbf{A}\mathbf{B}]^{-1} = \mathrm{tr}[\mathbf{I} + \mathbf{B}\mathbf{A}]^{-1},$$

for any matrices **A** and **B**. (The spectrum of **AB** is the same as that of **BA**.)

We now seek a minimum over all possible matrices **Q** such that

$$\int_{-\pi/T}^{\pi/T} \mathrm{tr}[\mathbf{I} + \bar{\mathbf{Q}}\mathbf{\Lambda}]^{-1}\mathbf{d}\omega = \min_{\mathbf{Q}} \int_{-\pi/T}^{\pi/T} \mathrm{tr}[\mathbf{I} + \mathbf{Q}\mathbf{\Lambda}]^{-1}\mathbf{d}\omega \tag{27}$$

subject to $\int_{-\pi/T}^{\pi/T} \mathrm{tr}\mathbf{Q}\mathbf{d}\omega = \text{constant}$.

Since $\mathbf{\Lambda}$ is real and nonnegative we define

$$\mathbf{M}(\omega) = \mathbf{\Lambda}^{1/2}(\omega)\mathbf{Q}(\omega)\mathbf{\Lambda}^{1/2}(\omega), \tag{28}$$

which is again diagonalized by unitary matrices $\mathbf{U}(\omega)$,

$$\mathbf{M} = \mathbf{U}\mathrm{dig}(\delta_1 \cdots \delta_N)\mathbf{U}^{\dagger}, \tag{29}$$

where $\delta_1 \cdots \delta_N$ are now the eigenvalues of **M**. Let the diagonal elements of **M** be $d_1 \cdots d_N$. We then obtain from (29)

$$d_i = \sum_{n=1}^{N} \delta_n |U_{in}|^2, \qquad i = 1 \cdots N. \tag{30}$$

This relationship is now used to prove that (27) is achieved when $\bar{\mathbf{Q}}$ is diagonal. Since the integrand in (27) is positive, it suffices to minimize the integral point by point.

Let $\mathbf{S}_d$ be the diagonal matrix formed from **M** by setting all off-diagonal entries to zero. From the definition of the trace we write

$$\mathrm{tr}[\mathbf{I} + \mathbf{M}]^{-1} = \sum_{n=1}^{N} \frac{1}{1 + \delta_n}$$

and

$$\mathrm{tr}[\mathbf{I} + \mathbf{S}_d]^{-1} = \sum_{n=1}^{N} \frac{1}{1 + d_n}.$$

If diagonal $\bar{\mathbf{Q}}$ renders the smallest trace, it must be shown that

$$\sum_{n=1}^{N} \frac{1}{1 + d_n} \leq \sum_{n=1}^{N} \frac{1}{1 + \delta_n}. \tag{31}$$

The proof of (31) is facilitated by the observation from (29) and (30) that

$$|U_{in}| \geq 0, \qquad i, n = 1 \cdots N$$

and

$$\sum_{i=1}^{N} |U_{in}|^2 = \sum_{n=1}^{N} |U_{in}|^2 = 1.$$

These are precisely the necessary and sufficient conditions that $2N$

numbers $\{d_i, \delta_i\}$ be related such that for any continuous convex function $\Phi(x)$ one has

$$\Phi(d_1) + \cdots + \Phi(d_N) \leq \Phi(\delta_1) + \cdots + \Phi(\delta_N). \tag{32}$$

(See Theorems 13 and 14 in Ref. 7, pp. 30–1.) Since only the diagonal entries in $\mathbf{Q}$ enter into the constraint, this result proves our assertion.

During the course of this research I discussed this assertion with my colleague Hans Witsenhausen, who supplied an elegant proof using Schur transformations. With his permission I reproduce his note to me in the Appendix.

Once we establish the fact that the optimum matrix $\mathbf{Q}$ is diagonal, we note from the definition that

$$\mathbf{Q} = \mathbf{G}\mathbf{G}^\dagger = \psi\mathbf{P}\mathbf{P}^\dagger\psi^\dagger = \text{diagonal}, \tag{33}$$

and since its entries are nonnegative, the form of the optimum transmitter matrix is immediate,

$$\begin{aligned} \mathbf{P}_0(\omega) &= \psi^\dagger(\omega)\mathbf{Q}^{1/2}(\omega)\mathbf{S}(\omega), \qquad |\omega| \leq \frac{\pi}{T} \\ &= [\mathbf{0}], \text{ elsewhere,} \end{aligned} \tag{34}$$

where $\mathbf{S}(\omega)$ is an arbitrary unitary matrix. Thus, there are an infinite number of $\mathbf{P}(\omega)$'s that yield minimum mean-squared error while yielding a fixed amount of total average transmitted power.

The additional problem of determining the optimum values of the diagonal elements q_n in $\mathbf{Q}$ is now easy since (26) can now be written as

$$F = \sum_{n=1}^{N} \int_{-\pi/T}^{\pi/T} \left[\frac{1}{1 + \lambda_n(\omega)q_n(\omega)} + \lambda q_n(\omega) \right] \mathrm{d}\omega, \tag{35}$$

which is easily minimized with respect to the positive quantities $\{q_n(\omega)\}$ using standard calculus of variation techniques, and the Lagrange multiplier is determined from the given power constraint. The minimization of (35) follows the same procedure as in the $N = 2$ case, treated in detail in Ref. 1.

V. CONCLUSIONS

Fallouts from solving some very special problems associated with digital communications over dually polarized radio channels yielded general results applicable to a wide range of communications situations. It appears that the class of minimization problems encountered in our formulations are well known to the mathematicians; if the engineers could only ask the right questions.

From a mathematical point of view, the optimum overall system has an end-to-end equivalent diagonal characterization. Once this diagonal

(direct) structure is determined, all other problems reduce to the well-known scalar case.

From an engineering point of view the optimum filter structures may provide valuable insights to the design of signal processors in the multiuser communications environment.

REFERENCES

1. N. Amitay and J. Salz, "Linear Equalization Theory in Digital Data Transmission Over Dually Polarized Fading Radio Channels," AT&T Bell Lab. Tech. J., *63*, No. 10 (December 1984), pp. 2215–59.
2. M. Kavehrad and J. Salz, private communication.
3. H. P. Kramer and M. V. Mathews, "A Linear Coding for Transmitting a Set of Correlated Signals," IRE Trans. Inform. Theory, *IT-2* (September 1956), pp. 41–6.
4. R. J. Pilc, "The Optimum Linear Modulator for a Gaussian Source Used With A Gaussian Channel," B.S.T.J., *48*, No. 9 (November 1969), pp. 3075–89.
5. L. H. Brandenberg and A. D. Wyner, "Capacity of the Gaussian Channel With Memory: The Multivariate Case," B.S.T.J., *53*, No. 5 (May–June 1974), pp. 745–78.
6. H. S. Witsenhausen, "A Determinant Maximization Problem Occurring in the Theory of Data Communication," SIAM J. Appl. Math., *29*, No. 3 (November 1975), pp. 515–22.
7. E. F. Beckenbach and Richard Bellman, *Inequalities*, Berlin, Heidelberg, New York: Springer-Verlag, 1965, pp. 30–1.
8. A. W. Marshall and I. Olkin, *Inequalities: Theory of Majorization and Its Applications*, New York: Academic, 1979.

APPENDIX

Yet Another Trace Minimization Problem

By H. S. Witsenhausen

Let (Ω, B, μ) be a measure space, and for each $\omega \in \Omega$ let $\Lambda(\omega)$ be an $N \times N$ diagonal matrix with real positive integrable diagonal entries.

Let $\mathbf{Q}$ denote a measurable function from Ω to nonnegative definite hermitian matrices, subject to

$$\int \mathrm{tr}\mathbf{Q}(\omega) \cdot \mathbf{d}\mu(\omega) = c. \tag{36}$$

One seeks the minimum, over all such $\mathbf{Q}$ of

$$\int \mathrm{tr}(\mathbf{I} + \mathbf{Q}(\omega)\Lambda(\omega))^{-1} \cdot \mathbf{d}\mu(\omega). \tag{37}$$

This problem is easily handled when $\mathbf{Q}$ is diagonal. The purpose of this Appendix is to show that the minimization can be reduced to this case.

Let $\mathbf{Q}^d$ denote the diagonal matrix obtained from $\mathbf{Q}$ by replacing all off-diagonal elements by zero.

Theorem: *If* $\mathbf{Q}(\cdot)$ *satisfies the conditions of the problem, then* $\mathbf{Q}^d(\cdot)$ *also does and gives* (37) *no higher value.*

Proof: Obviously, $\mathbf{Q}^d$ is hermitian, nonnegative definite and gives the same value in (36). Now (37) can be written

$$\int \operatorname{tr}(\mathbf{I} + M(\omega))^{-1} \cdot \mathbf{d}\mu(\omega), \tag{38}$$

where

$$\mathbf{M}(\omega) = \mathbf{\Lambda}^{1/2}(\omega)\mathbf{Q}(\omega)\mathbf{\Lambda}^{1/2}(\omega) \tag{39}$$

is hermitian, nonnegative definite.

We have

$$\mathbf{M}^d(\omega) = \mathbf{\Lambda}^{1/2}(\omega)\mathbf{Q}^d(\omega)\mathbf{\Lambda}^{1/2}(\omega). \tag{40}$$

Thus it is enough to show that (38) cannot increase when $\mathbf{M}$ is replaced by $\mathbf{M}^d$, which we show for each fixed ω.

Let $\lambda_1, \cdots, \lambda_n$ be the eigenvalues of $\mathbf{M}$, and let $d_1, \cdots, d_n$ be the diagonal entries of M that are the eigenvalues of $\mathbf{M}^d$.

$$\operatorname{tr}(\mathbf{I} + \mathbf{M})^{-1} = \sum_{i=1}^{n} \frac{1}{1 + \lambda_i}. \tag{41}$$

$$\operatorname{tr}(\mathbf{I} + \mathbf{M}^d)^{-1} = \sum_{i=1}^{n} \frac{1}{1 + d_i}. \tag{42}$$

The right side of (41) is a convex symmetric function of $(\lambda_1, \cdots, \lambda_n)$. Hence it is Schur convex. (That is, $f(\mathbf{S}\lambda) \leq f(\lambda)$ for doubly stochastic $\mathbf{S}$.)

As observed by Schur, from the unitary relationship of $\mathbf{M}$ with its diagonal form

$$\mathbf{M} = \mathbf{U}\ \operatorname{diag}(\lambda_1, \ldots, \lambda_n)\mathbf{U} \tag{43}$$

(see Ref. 8), it follows that

$$\mathbf{d} = \mathbf{S}\lambda \tag{44}$$

with doubly stochastic $\mathbf{S}(S_{ij} = |u_{ij}|^2)$.

Thus,

$$\sum_{i=1}^{n} \frac{1}{1 + d_i} \leq \sum_{i=1}^{n} \frac{1}{1 + \lambda_i}, \tag{45}$$

which was to be proved.

These two quantities, sometimes referred to as efficiency indices, will be used to compare the performance of the various equalization methods.

AUTHOR

Jack Salz, B.S.E.E., 1955, M.S.E., 1956, and Ph.D. (Electrical Engineering), 1961, University of Florida; AT&T Bell Laboratories, 1961—. Mr. Salz first worked on the electronic switching system. Since 1968 he has supervised a group engaged in theoretical studies in data communications and is currently a member of the Network Systems Research Department. During the academic year 1967–68, he was on leave as Professor of Electrical Engineering at the University of Florida. He was a visiting lecturer at Stanford University in Spring 1981 and a visiting MacKay Lecturer at the University of California, at Berkeley, in Spring 1983.

AT&T Technical Journal
Vol. 64, No. 6, July–August 1985
Printed in U.S.A.

Tone Location by Cyclotomic Filters

By D. HERTZ,* R. P. KURSHAN,† D. MALAH,* and J. T. PEOPLES‡

(Manuscript received July 11, 1984)

In this paper we present a tone location system that estimates the frequency of an input tone through additions and comparisons alone. The system uses "cyclotomic" filters (which operate without multiplications), requiring fewer operations than with a conventional Discrete Fourier Transform (DFT) entailing multiplications. In the system presented here, an input tone is first transformed to yield two quadrature tones, which are then digitized. Processing occurs in successive stages at successively reduced sampling rates. During each decimation stage, the system is configured to provide symmetric coverage of a subband in which the tone has been located at the previous stage. Simulations demonstrate that for the case studied, an input signal-to-noise ratio (SNR_i) in excess of 10 dB yields an output signal-to-noise ratio (SNR_o) that is close (within 0.3 dB) to the maximum attainable SNR_o, where SNR_o is measured in terms of the reduction in frequency uncertainty. Enhanced resolution is demonstrated at the expense of the number of computations, while holding the number of decimation stages constant, by using small DFTs in place of the cyclotomic filters. This method still utilizes fewer computations than a conventional DFT (with the same number of frequency cells), with approximately the same performance in the case of low noise. Thus, this alternative method is useful when circumstances prohibit using a single, large DFT.

* Technion-Israel Institute of Technology, Haifa, Israel. This paper is derived from the M.Sc. thesis of D. Hertz, published in 1979, written under the direction of D. Malah and R. P. Kurshan (while the latter was visiting the Technion in 1976–7). Part of the work was completed while D. Malah was visiting AT&T Bell Laboratories in 1979–81.
† AT&T Bell Laboratories. ‡ AT&T Bell Laboratories; present affiliation Bell Communications Research, Inc.

I. INTRODUCTION

In many diverse applications, it is necessary to detect and locate a signal appearing within selected frequency bands, particularly a signal comprised of a single tone. This is tantamount to estimating the frequency of a tone that may appear randomly in any band. Such detection and estimation are generally accomplished in conventional analog systems, using a bank of filters tuned to different, narrowband portions of the spectrum or using a single filter that is effectively swept across the bands of interest. Associated with such techniques, however, are the usual problems of analog processors, including unpredictability due to inherent variability of system components. A discrete-time technique is described by Cappelini et al.,[1,2] wherein a given frequency band is partitioned into subbands for detection purposes. The partition into subbands is achieved through a decimation approach, using a single, fixed, low-pass digital filter at each decimation stage. In a variety of applications, however, when it is known that the given input signal contains, at most, a single spectral line in the frequency range of interest (e.g., in M-ary FSK demodulation[3] and Touch-Tone telephony[4]), this method possesses inherent disadvantages. First, since general filtering is effected at each decimation stage, numerous multiplications and additions must be performed during the filtering operations of each stage. Second, a large amount of memory is required to store samples from the geometrically increasing number of iterated signals. These disadvantages are substantially reduced with a Cyclotomic Tone Location System (CTLS).[5-8] Only the CTLS of Ref. 5 is presented here, since it is simpler than the CTLS of Refs. 6 through 8, and we wish to apply this same idea to a DFT Tone Location System (FTLS) as well, described in Section IV. The FTLS, as compared with conventional DFT implementations,[9,10] trades performance in the presence of noise for reduced implementational complexity.

The CTLS incorporates digital filters utilizing additions alone, thereby eliminating the customary computational load associated with multiplications. Figure 1 is a block diagram of the CTLS. Referring to Fig. 1, the input tone, comprising, say, a single frequency located randomly within a band 0 to $f_s/4$, is first transformed by the Hilbert network to yield a complex tone composed of two tones in quadrature relationship. These two tones correspond to phase-shifted versions of the input tone. The complex tone is initially sampled by the digitizer at a rate of f_s and stored in the buffer. Then, the complex tone and its frequency-shifted versions, from the frequency-shifting unit, are processed by the first-order recursive filter unit. The filters are derived from the set of cyclotomic filters and have only a single resonance in the frequency range up to one-half the sampling rate. The filters are

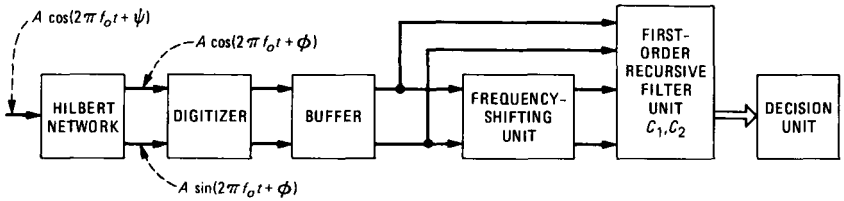

Fig. 1—Block diagram of the CTLS.

arranged so that the resonances associated with the filters and frequency-shifted versions symmetrically cover a band of frequencies including the input tone frequency. Location of the subband containing the tone is achieved in the decision unit by comparing the magnitudes of the various filter outputs to each other after a fixed number of samples have been processed.

It is assumed from here on that *the tone is known to be present.* The problem of detecting the presence of a tone will be commented on later in this paper. The CTLS locates the tone using a multistage process. At the first stage, using the first-order recursive filter unit, which symmetrically covers the band $(0, f_s/4)$, the CTLS unambiguously locates the tone either in $(0, f_s/8)$ or in $(f_s/8, f_s/4)$. Once the tone has been located within a single subband, sampling rate reduction, or decimation, by a factor of two is effected.

This particular choice of the sampling rate reduction ratio and subband width precludes additional spectral lines from appearing within the subband containing the tone. The filters are now reconfigured at the reduced sampling rate to again achieve symmetrical placement of the filter resonances across the previously isolated subband of width $f_s/8$ containing the tone. The process of frequency shifting and filtering by the array is then repeated.

The frequency subbands utilized for resolution at the output of this second stage are each of width $f_s/16$. Again, the subband containing the tone is isolated, and another decimation stage is effected. The processing continues in this manner until the desired frequency resolution has been achieved. Moreover, a minor modification to the CTLS enables the system to test for a tone in any one of the other three bands [rather than $(0, f_s/4)$], i.e., $[kf_s/4, (k+1)f_s/4]$, $k = 1, 2, 3$, provided k is known to the CTLS.

The FTLS is an extension of the CTLS in the following way. Basically, the input tone to the FTLS is comprised of a frequency, located randomly within the band 0 to $f_s/2$, and is converted to a complex tone. The quadrature tones are both initially sampled at a rate of f_s, and then N samples of the complex tone are processed by an M-point DFT ($M = 2^m$, $N < M$ is mandatory, and the N samples

are padded by $M - N$ zeros). The modulus of the M-point DFTs are further processed. As in the CTLS, the processing is done in successive stages at successively reduced sampling rates. During each decimation stage, the system is configured to provide symmetric coverage of a subband in which the tone has been located in the previous stage.

At each decimation stage the pertinent band is partitioned into $M/2$ subbands [with S stages the initial band will be partitioned into $(M/2)^S$ bands]. A minor modification to the FTLS enables the system to test for a tone in the other band, i.e., $(f_s/2, f_s)$, provided the FTLS knows in which of the two subbands the tone is present. For $N = 2, 3$, and $M = 4$ this reduces to a CTLS, except for the sampling rate, which is now halved.

The organization of the paper is as follows: Section II presents basic relations and a detailed description of the CTLS; Section III gives simulation results associated with the CTLS; Section IV presents a detailed description of the FTLS; and Section V presents the conclusions.

II. CTLS OPERATION PRINCIPLES

For clarity of exposition, we first present an overview of the properties of the first-order recursive filters utilized here. Next, we discuss in detail the time-domain and frequency-domain characteristics of one first-order filter (designated C_1), treated as exemplary of the remaining filters of interest (designated C_2, C_{4p}, and C_{4m}), to illustrate fundamental concepts helpful to fully comprehend the overall CTLS. Finally, we describe the technique for exploiting the properties of the individual filters to form a composite tone detection system.

2.1 Cyclotomic filters

The properties of the cyclotomic filters discussed herein are presented in greater detail in Kurshan and Gopinath[11] and Hertz.[8] Cyclotomic filters are a class of digital filters having only poles in the transfer function and, moreover, each pole lies on the unit circle. This means that the filters are inherently unstable and are not suitable for conventional filtering operations, which require the processing of numerous sequential samples. In fact, these filters behave more like resonators and it is this property that can be beneficially utilized for tone detection. The salient advantage of this type of resonating filter is that the filters of primary interest exhibit nonzero coefficient values $(\pm 1, \pm j)$ having a modulus of one. This implies that multiplications of samples by filter coefficients reduce to simple addition, subtraction, and signal interchange operations and, significantly, arithmetic errors such as round-off and truncation errors are eliminated.

A cyclotomic filter may be described in terms of a linear recursion

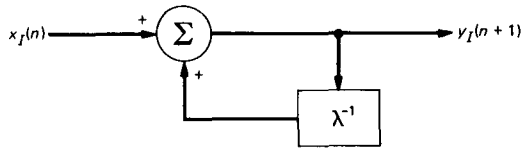

Fig. 2—Cyclotomic digital filter C_1 in block diagram form.

relation whose characteristic polynomial is a cyclotomic polynomial. For example, for a first-order digital filter represented by the Linear Difference Equation (LDE)

$$y_I(n+1) = y_I(n) + x_I(n), \tag{1}$$

where $x_I(n)$ and $y_I(n)$ are inphase input and output sequence elements, respectively, corresponding to the nth sample, then the characteristic equation is given by the polynomial $\lambda - 1$ (as derived from $y_I(n+1) - y_I(n) = 0$). This polynomial is cyclotomic and has the designation $C_1(\lambda)$ (or C_1 for simplicity): $C_1(\lambda) = \lambda - 1$. Similarly, the cyclotomic polynomial $C_2(\lambda) = \lambda + 1$ yields a digital filter described by the LDE

$$y_I(n+1) = -y_I(n) + x_I(n). \tag{2}$$

Other filters of special interest include two first-order, complex filters derived as the roots of the second-order cyclotomic polynomial $C_4(\lambda) = \lambda^2 + 1$. These filters also have roots on the unit circle and are given by (with $j = \sqrt{-1}$) $C_{4p}(\lambda) = \lambda - j$ and $C_{4m}(\lambda) = \lambda + j$; they have the following LDE representations, respectively:

$$y_I(n+1) = jy_I(n) + x_I(n) \tag{3}$$

and

$$y_I(n+1) = -jy_I(n) + x_I(n). \tag{4}$$

Figure 2 depicts the C_1 digital filter in block diagram form. Similar block diagrams can be derived for the other first-order filters.

2.2 Filter characteristics

To elucidate the desired characteristics obtained by combining cyclotomic-derived filters into a system architecture, we first present the response of a general filter to an input tone having a randomly distributed phase component. The input tone is presumed to have the analog form $A\cos(2\pi ft + \varphi)$, where φ is the random phase variable, A is the amplitude, and f is the tone frequency.

The impulse response sequence of the general recursive filter is represented by $\{h(k)\}$, where $k \geq 0$. The output sequence elements may then be obtained from the convolutional relationship

$$y_I(n) = \sum_{k=0}^{n} x_I(k)h(n-k), \tag{5}$$

where $\{x_I(k)\}$ is the input tone sequence obtained by sampling $A\cos(2\pi ft + \varphi)$, $t \geq 0$, at the rate f_s, that is,

$$x_I(k) = A\cos(k\nu + \varphi), \qquad k \geq 0, \tag{6}$$

where

$$\nu = 2\pi f/f_s. \tag{7}$$

Substituting (6) into (5) gives

$$y_I(n) = \sqrt{\alpha_n^2 + \beta_n^2}\cos\left[\tan^{-1}\left(\frac{\beta_n}{\alpha_n}\right) + \varphi\right], \tag{8}$$

where

$$\alpha_n = \mathrm{Re}\left[\sum_{k=0}^{n} Ae^{jk\nu}h(n-k)\right], \tag{9}$$

$$\beta_n = \mathrm{Imag}\left[\sum_{k=0}^{n} Ae^{jk\nu}h(n-k)\right], \tag{10}$$

and the operators denoted "Re" and "Imag" produce the real and imaginary parts of the bracketed part of eqs. (9) and (10), respectively.

Since φ occurs randomly within the interval $(0, 2\pi)$, comparison of $|y_I(n)|$ to a threshold may yield deleterious results due to the dependence of y_n on φ. However, by utilizing the first-order filters in pairs (either actually or on a time-shared basis), the undesirable modulation effects of the random phase component may be eliminated.

This is achieved by forming a new sample sequence $\{x_Q(k)\}$, found by sampling the quadrature tone $A\sin(2\pi ft + \varphi)$, which may be derived through a Hilbert transform operation on the original or inphase input tone. The new sequence elements are given by

$$x_Q(k) = A\sin(k\nu + \varphi), \qquad k \geq 0. \tag{11}$$

If $\{x_Q(k)\}$ is processed by a recursive filter identical to the one that processes $\{x_I(k)\}$, then the new output sequence $\{y_Q(n)\}$ has elements

$$y_Q(n) = \sqrt{\alpha_n^2 + \beta_n^2}\sin\left[\tan^{-1}\left(\frac{\beta_n}{\alpha_n}\right) + \varphi\right]. \tag{12}$$

A squaring operation on both eqs. (8) and (12), followed by a summation and square-root operation, yields an output $\sqrt{\alpha_n^2 + \beta_n^2}$, which is independent of φ.

For future discussion, it is convenient, as exemplified by the form of eqs. (9) and (10), to define a complex input tone having sample

values $Ae^{j(k\nu+\varphi)}$, and a corresponding output sequence $\{z_n\}$ having complex element values

$$z_n = \sum_{k=0}^{n} Ae^{j(k\nu+\varphi)}h(n-k). \tag{13}$$

The magnitude or modulus of each element of $\{z_n\}$ is then given by

$$|z_n| = |\sum_{k=0}^{n} Ae^{jk\nu}h(n-k)| = \sqrt{\alpha_n^2 + \beta_n^2}. \tag{14}$$

As hereinafter utilized, the two-filter device characterized by substantially identical filters $C_i(i = 1, 2, 4p \text{ or } 4m)$, which processes inphase and quadrature samples of an input signal in pairs, is a basic or fundamental element of the CTLS.

Whereas the above discussion has focused primarily on sequence domain manipulations, it is helpful to visualize these manipulations in the frequency domain. Moreover, whereas the discussion was couched in terms of generalized impulse responses, particularly pertinent to the subsequent discussion are the frequency domain responses of filters C_1, C_2, C_{4p}, and C_{4m}. The filter C_1, having impulse elements $h(n) = 1$, $n \geq 0$, is treated as exemplary.

Utilizing now the notation $z(C_1, n, \nu)$ to distinguish sequence elements of $\{z_n\}$ so as to explicitly set forth the dependence upon C_1, n and ν, we obtain the following by substituting $h(n) = 1$ into eq. (14):

$$|z(C_1, n, \nu)| = A\,|\sum_{k=0}^{n} e^{jk\nu}|$$

or

$$|z(C_1, n, \nu)| = A\left|\frac{\sin\left(\frac{n+1}{2}\right)\nu}{\sin\frac{\nu}{2}}\right|. \tag{15}$$

In addition, because the impulse response of C_2 is $(-1)^n$, $n \geq 0$,

$$|z(C_2, n, \nu)| = |z(C_1, n, \nu + \pi)|. \tag{16}$$

Figure 3 shows plots of $|z(C_1, n, \nu)|$ and $|z(C_2, n, \nu)|$ over the range (0 to π) for $n = 3$, that is, four samples corresponding to $n = 0$, 1, 2, and 3 have been processed. The resonating feature of the filters is apparent. Filter C_1 is symmetric with respect to $\nu = 0$, whereas C_2 is symmetric about $\nu = \pi$, and both are periodic with period 2π. Since $\nu = 2\pi f/f_s$, $\nu = \pi$ corresponds to a frequency f, which is one-half the sampling rate. Although the filter response has been illustrated with four samples, the filter may also be operated with two, three, five, six,

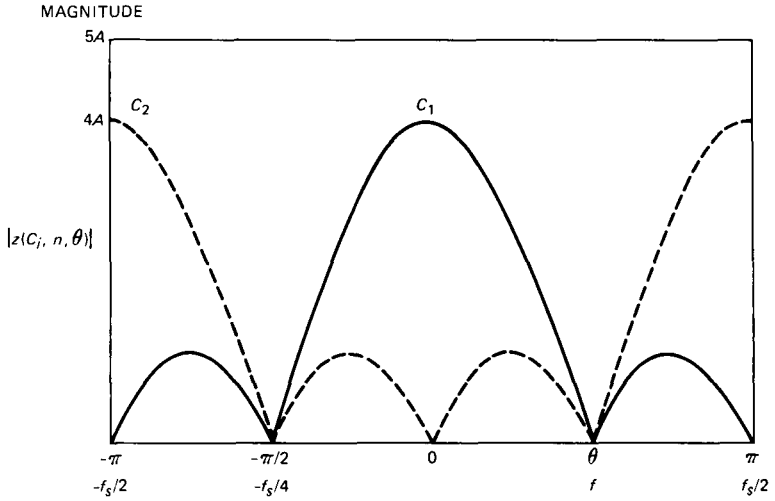

Fig. 3—Responses of filter pairs C_1 and C_2, each processing real and imaginary sampled tones in parallel, over the range from 0 to one-half of the sampling rate with $N = 4$ samples.

or seven samples. If more than seven samples are used, the main lobes of adjacent filter responses do not intersect. In fact, simulations reveal some enhancement in the signal-to-noise performance when more than four (but fewer than seven) samples are processed.

In a similar manner, the following relations may also be derived:

$$|z(C_{4p}, n, \nu)| = A \left| \frac{\sin\left[\left(\frac{n+1}{2}\right)\left(\nu - \frac{\pi}{2}\right)\right]}{\sin\left[\frac{\left(\nu - \frac{\pi}{2}\right)}{2}\right]} \right| \tag{17}$$

and

$$|z(C_{4m}, n, \nu)| = A \left| \frac{\sin\left[\left(\frac{n+1}{2}\right)\left(\nu + \frac{\pi}{2}\right)\right]}{\sin\left[\frac{\left(\nu + \frac{\pi}{2}\right)}{2}\right]} \right|. \tag{18}$$

Because of the manner in which C_{4p} and C_{4m} are related to C_1,

$$\left|z\left(C_{4p}, n, \nu + \frac{\pi}{2}\right)\right| = \left|z\left(C_{4m}, n, \nu - \frac{\pi}{2}\right)\right| = |z(C_1, n, \nu)|. \tag{19}$$

Figure 4 shows plots of $|z(C_{4p}, n, \nu)|$ and $|z(C_{4m}, n, \nu - \pi)|$ for the same parameters as Fig. 3. Since cyclotomic filters have poles on the unit circle, their responses blow up. However, they can be used only because the input signal is time limited, hence the composite response due to the sinusoidal input can be examined and leads to eqs. (15) through (18).

From the plots of Figs. 3 and 4, we conclude that the filter response from each two-filter device comprising identical filters $C_i (i = 1, 2, 4p$ or $4m)$ has only a single resonance in the frequency range up to one-half of the sampling frequency. The CTLS exploits these filter pairs by covering the frequency band from 0 to $f_s/2$ (ν from 0 to π) in symmetric fashion. Such an arrangement is depicted in Fig. 5a. Since C_{4p} and C_{4m} are merely frequency-shifted versions of C_1 and it appears that C_{4p} and C_{4m} require complex manipulations, it is important to determine if a modified, real sequence can serve as an input to a C_1 filter to produce an output equivalent to a C_{4p} or C_{4m} filter output.

Phase shifting by $\pm\pi/2$ in the frequency domain is equivalent to introducing modulation factors in the sequence (sampled time) domain of the form $\{e^{\pm jk\pi/2}\}$. Thus, if the complex input sequence is modified by the modulation sequence, a new sequence having element values

$$Ae^{j[k(\nu \pm \pi/2)+\varphi]} \tag{20}$$

gives rise to an output corresponding to C_{4p} or C_{4m}, as appropriate. The inphase and quadrature sequences associated with this complex input sequence become, respectively,

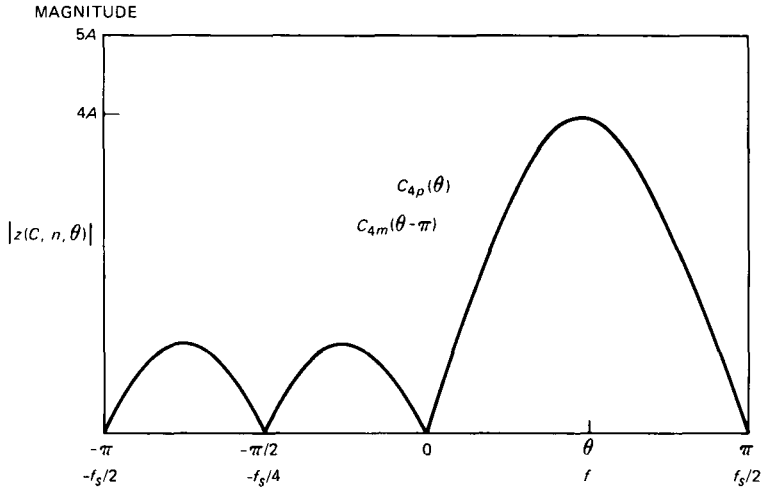

Fig. 4—Responses of complex, recursive filter pairs C_{4p} and C_{4m} in the same scale and over the same range of frequency as in Fig. 3.

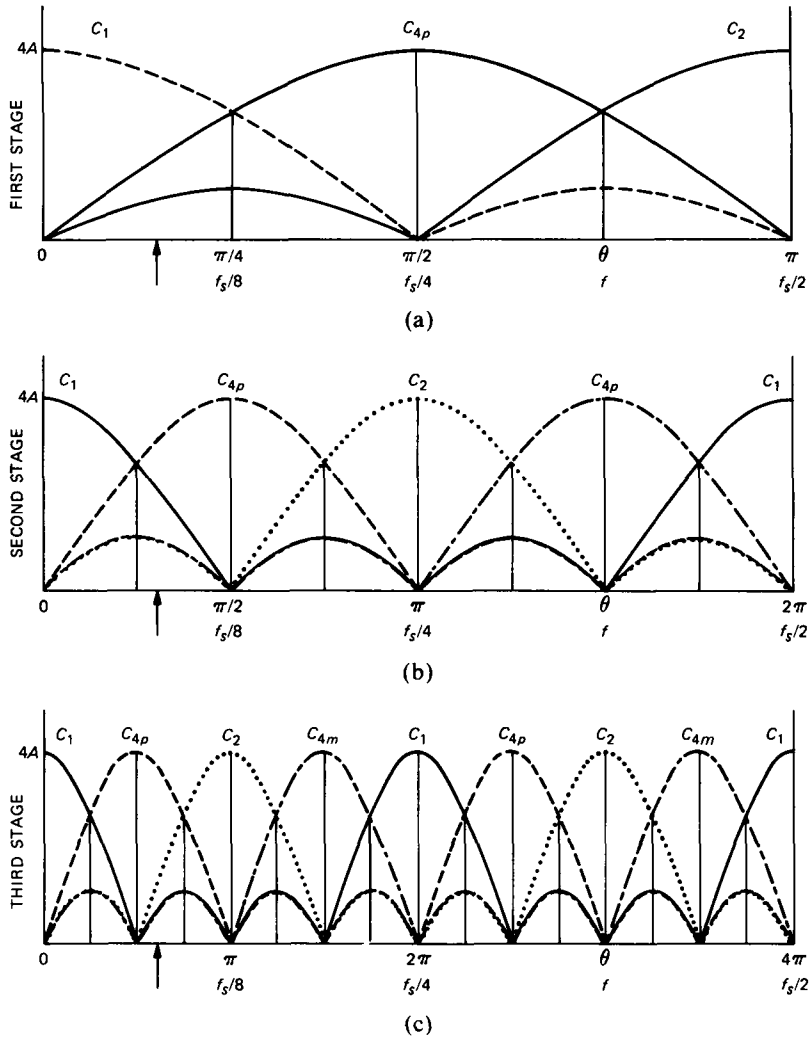

Fig. 5—(a) Arrangement of three first-order recursive filters that cover the frequency band from 0 to one-half of the sampling rate. (b) Arrangement of four recursive filters that cover the band from 0 to one-half of the initial sampling rate and are symmetric over the four subbands shown in Fig. 5a. (c) Arrangement of eight recursive filters that cover the band from 0 to one-half of the initial sampling rate and are symmetric over the eight subbands shown in Fig. 5b.

$$A\cos(k\nu + \varphi)\cos(k\pi/2) \mp A\sin(k\nu + \varphi)\sin(k\pi/2) \qquad (21)$$

and

$$A\sin(k\nu + \varphi)\cos(k\pi/2) \pm A\cos(k\nu + \varphi)\sin(k\pi/2). \qquad (22)$$

Since k is a nonnegative integer, the shifted inphase sequence reduces

to a sequence that is periodic of period four having element values for $k = 0, 1, 2$ and 3 of [from eq. (21)]:

$$A\cos(k\nu + \varphi);\quad \mp A\sin(k\nu + \varphi);$$
$$-A\cos(k\nu + \varphi);\quad \pm A\sin(k\nu + \varphi). \quad (23)$$

Similarly, the shifted quadrature sequence has elements for $k = 0, 1, 2, 3$ [from eq. (22)] of:

$$A\sin(k\nu + \varphi);\quad \pm A\cos(k\nu + \varphi);$$
$$-A\sin(k\nu + \varphi);\quad \mp A\cos(k\nu + \varphi). \quad (24)$$

Examination of eqs. (23) and (24) suggests that the operation of normalized frequency shifting by $\pm\pi/2$, rather than occurring through frequency-domain manipulations, may be straightforwardly implemented in the sequence or sample domain merely by interchanging and changing signs of the inphase and quadrature inputs to a filter pair, when appropriate. Because of the form of eq. (20), such an implementation may be referred to as a modulus-one multiplier ($j^{\pm k}$) or frequency shifter.

Figure 6 is a block diagram of the modulus-one multiplier for the case of a $-\pi/2$ frequency shift (C_{4p}). The inputs to this unit are the original inphase and quadrature sequence elements. The operations of sign changing and line interchanging occur within this unit, as depicted for $k = 0, 1, \ldots, 4, \ldots$. The frequency-shifted, inphase, and quadrature sequence elements, respectively, are fed to two identical C_1 filters whose outputs are squared, summed, and square rooted. Finally, this unit provides the response described above by C_{4p}. Note that the operations needed to compute the modulus $\sqrt{x^2 + y^2}$ can be simplified

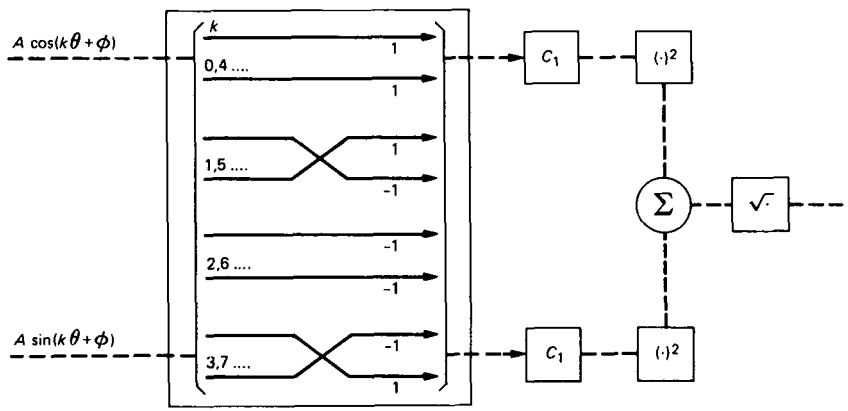

Fig. 6—Block diagram of a modulus-one multiplier for the case of a $-\pi/2$ frequency shift (C_{4p}).

by using known approximations to the modulus (see Refs. 12 through 14). An example is the one given by

$$\sqrt{x^2 + y^2} \simeq \text{Max}(|x|, |y|) + \alpha \text{ Min}(|x|, |y|). \tag{25}$$

α is a scalar multiplier. In Refs. 5 through 7 we used $\alpha = 0.25$, so that multiplication by α corresponds to two shift operations. The choice of $\alpha = 0.25$ causes only a small degradation in performance, as has been noted in simulations.

Figures 5b and 5c depict how each of the two subbands in the range 0 to $\pi/2$ of Fig. 5a may be further partitioned to isolate the tone of interest. Basically, the subbands are subdivided into second-stage subbands by reducing the sampling rate and reconfiguring the filter array within each subband of interest. For instance, the first-stage subband labeled C_1 in Fig. 5a has been subdivided by reducing the sampling rate by a factor of two and covering the old subband by C_1, C_{4p}, which effects two second-stage subbands symmetrically dispersed across the original subband. Further sampling rate reduction by a factor of two results in the partition of Fig. 5c. The configuration and covering of Fig. 5b occurs within each subband during each stage of decimation after the first stage.

To understand how the given input tone can be isolated by processing with consecutive stages of decimation, the steps in processing a single tone of frequency f_0 are now considered. For the complex tone initially sampled at a rate f_s, spectral lines occur in the digital spectrum at $f_0 + kf_s$, $k = 0, \pm 1, \ldots$. The sampling rate is chosen so that the tone falls within the range 0 to $f_s/4$ ($0 < f_0 < f_s/4$); thus the tone may be unambiguously determined to fall within one of the subbands or cells $(0, f_s/8)$ or $(f_s/8, f_s/4)$, by processing the outputs from the filter array or bank configured as C_1, C_{4p}. This is basically accomplished by comparing each filter output to another.

If the complex tone samples are now decimated by a factor of two, that is, only every second value from the original set of samples is retained, then spectral lines appear at $f_0 + kf_s/2$, $k = 0, \pm 1, \ldots$. By selecting the 2:1 ratio between initial sampling rate and reduced sampling rate, and by selecting cell widths of $f_s/8$ for the first stage of sampling, no additional spectral components fall within the original subband containing baseband spectral line f_0. This is true, even though aliasing occurs, because the judicious selection of cell width and reduced sampling rate precludes aliased spectral lines from appearing in the subband containing the spectral line of interest.

The process described with respect to the decimation by a factor of two may continue until the desired resolution (final cell width) is achieved. In Figs. 5a through c three stages of processing are exemplified. The tone will thus be resolved to a cell of width $f_s/32$.

For example, say that $2(f_s/32) \leq f_0 \leq 3(f_s/32)$ (see also the arrows in Figs. 5a through c). At the first stage (Fig. 5a), the output of C_1 is compared to the output of C_{4p}; since "$|C_1| > |C_{4p}|$" it is concluded that the tone is located in $0 \leq f_0 \leq f_s/8$. At the second stage (Fig. 5b), the output of C_1 is compared to the output of C_{4p}, and since "$|C_1| < |C_{4p}|$" it is concluded that the tone is in $f_s/4 \leq f_0 \leq f_s/8$. At the final stage, stage three (Fig. 5c), the output of C_{4p} is compared to the output of C_2, and since "$|C_{4p}| > |C_2|$" it is concluded that the tone is in $f_s/16 \leq f_0 \leq 3f_s/32$, which is the correct presumed tone's location.

From the description with respect to the band from 0 to $f_s/4$, it is also apparent that a tone in the bands $(kf_s/4, (k+1)f_s/4)$, $k = 1, 2, 3$ could be processed in an analogous manner, provided k is known to the CTLS and only a single tone is present.

III. CTLS PERFORMANCE

In the previous section only the principles of operation of the CTLS were presented, and no consideration was given to the presence of noise in which the tone is usually embedded.

To combat the noise we propose two methods, based on soft decision and hard decision, respectively. To examine the performance of the CTLS, computer simulations were performed. In the simulations the location of the tone was initially set in the interval $(0, f_s/4)$ and was resolved by the CTLS into one of 64 cells. In each experiment 256 complex data words were processed. At each stage, the filters were operated for a small number of samples ($2 \leq N \leq 7$) as compared with the number of data words (256). Therefore, the filter operation was repeated at each stage (without overlapping the data), exhausting the data.

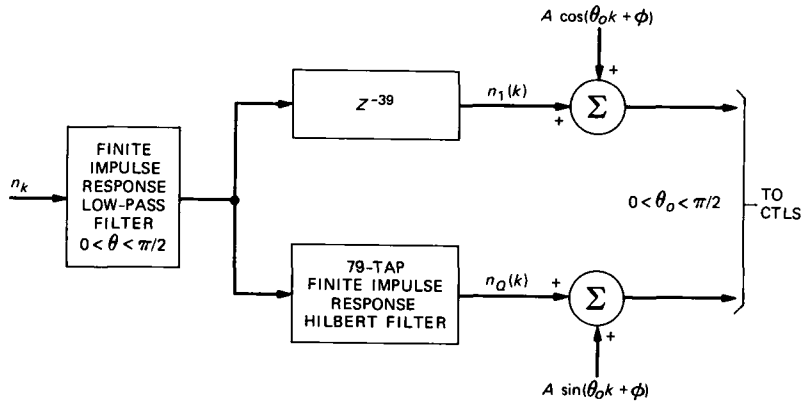

Fig. 7—Block diagram of the configuration for generating the input noisy tone to the CTLS.

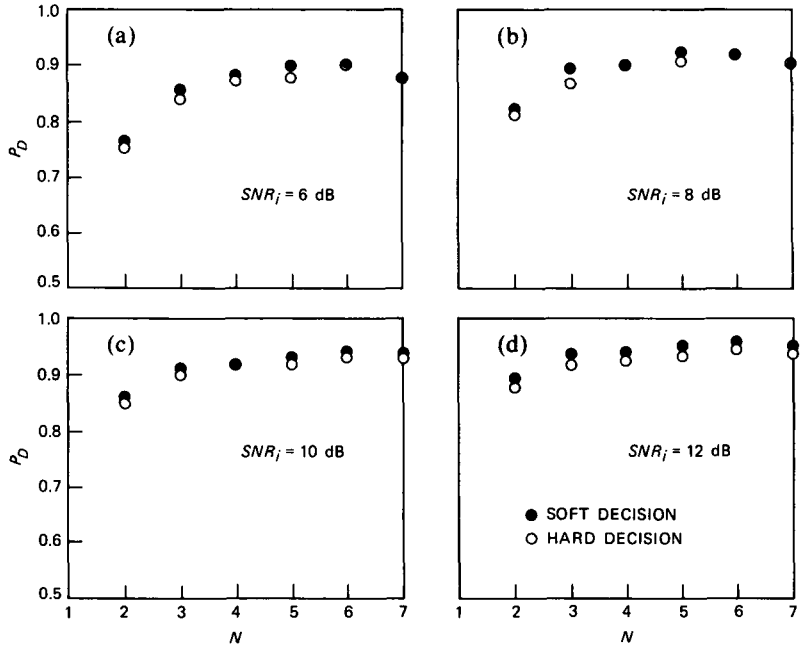

Fig. 8—Probability of correct tone location vs. number of samples; the filters are operated at different input SNR_i values.

With the hard-decision method, the CTLS uses (at each stage) the maximal output of the filters (over all repetitions). With the soft-decision method, the average (over all repetitions) of the filter's output at each stage is used.

Figure 7 is a block diagram of the operations carried out to generate the noisy complex digital tone that was fed to the CTLS. $\{n_k\}$ is a zero mean white ($E\{n_k n_j\} = \sigma^2 \delta_{kj}$) Gaussian sequence, which was low-pass filtered to eliminate out-of-band noise.

The simulations were carried out for different values of SNR_i(6, 8, 10, 12 dB):

$$SNR_i \triangleq \frac{A^2}{E\{n_I^2(k) + n_Q^2(k)\}}, \tag{26}$$

where E denotes the expectation operator. Figure 8(a through d) presents simulation results for the probability of locating the input tone in the correct cell as a function of the number of samples for which the filters are operated ($2 \leq N \leq 7$).

Another performance measure used in our simulations is the output signal-to-noise ratio (SNR_o), which gives the reduction in frequency uncertainty,[10] that is,

$$SNR_o = \frac{\text{var}(\nu_o)}{\text{var}(\nu_o - \hat{\nu}_o)}. \tag{27}$$

In (27) ν_o denotes the uniformly distributed input-normalized frequency (in the range 0 to $\pi/2$), and $\hat{\nu}_o$ is its estimate at cell width.

It is known[10] that when no errors are made in assigning the input signal to a cell, then

$$\max SNR_o = (N_c - 1)^2, \tag{28}$$

which gives 36.12 dB for $N_c = 64$, that is, 64 cells. Figure 9(a through d) shows the computer simulation results obtained for SNR_o as a function of the number of samples at which the filters were operated ($2 \leq N \leq 7$), at different SNR_i values (in the range of 6 to 12 dB).

From the simulation results in Figs. 8 and 9, we conclude the following:

1. The soft-decision method is superior to the hard-decision method.
2. The filters should operate with $N = 6$ samples.

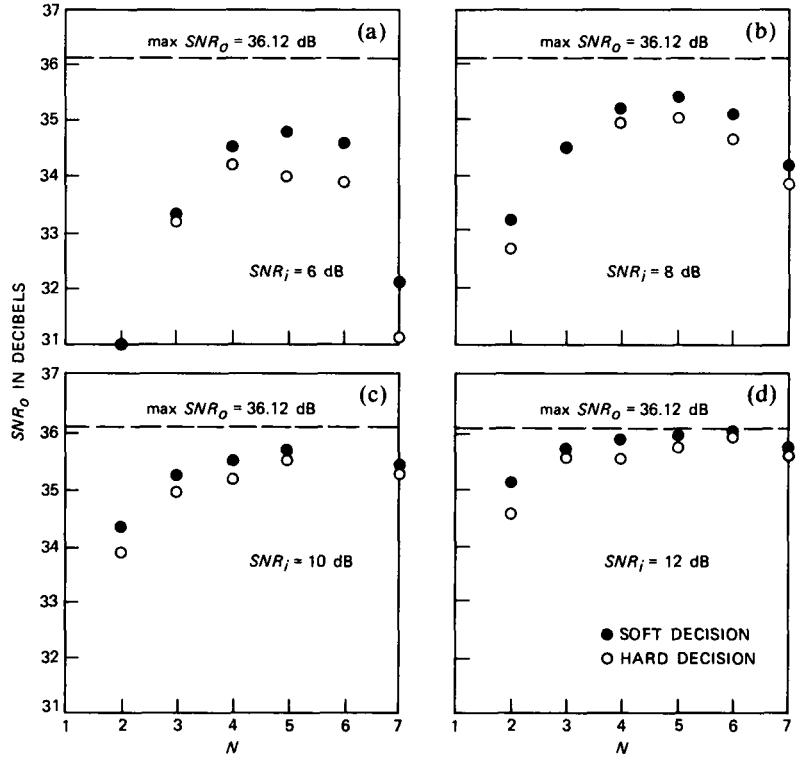

Fig. 9—Output signal to noise ratio (SNR_o) vs. number of samples; the filters are operated at different input SNR_i values.

3. For $SNR_i \geq 10$ dB and in conjunction with (1) and (2), the probability of locating the tone in the correct cell is in excess of 95 percent, and SNR_o is smaller than max SNR_o by less than 0.3 dB.

IV. DFT TONE LOCATION SYSTEM

In this section we present the DFT Tone Location System (FTLS). Let $\{x_i\}_{i=0}^{N-1}$ be N samples of the complex tone; then

$$X_k = DFT\{x_i\} = \sum_{i=0}^{N-1} x_i e^{-j\frac{2\pi}{M}ki}, \tag{29}$$

i.e., $x_i = 0$ for $i = N, N+1, \ldots, M-1 (M > N$ is mandatory), and

$$A_k = |X_k|, \qquad k = 0, 1, \ldots, M-1. \tag{30}$$

It can be easily demonstrated that

$$A_k = |y_{N-1}(k)|, \tag{31}$$

where

$$y_{l+1}(k) = e^{j\frac{2\pi}{M}k} y_l(k) + x_l,$$

$$y_o(k) = 0, \qquad l = 0, 1, \ldots, N-1. \tag{32}$$

Therefore, $z(C_i, N-1, \nu)$, $i = 1, 2, 4p, 4m$ [see eqs. (15) through (18)] are merely particular samples of A_k, i.e., A_o, $A_{M/2}$, $A_{M/4}$, $A_{3M/4}$. Similar to the derivations of (15) through (18), we get

$$A_k = A \left| \frac{\sin\left[\frac{N}{2}\left(\nu - \frac{2\pi}{M}k\right)\right]}{\sin\frac{1}{2}\left(\nu - \frac{2\pi}{M}k\right)} \right|, \tag{33}$$

where A and ν are the tone's amplitude and normalized frequency, respectively.

The operation principles of the FTLS are now explained. The input tone, which is comprised of a frequency located randomly within the band 0 to $f_s/2$, is converted into a complex tone. The quadrature tones are both initially sampled at a rate of f_s and then N samples of the complex tone are processed by an M-point DFT ($M = 2^m$, $N < M$, and the N samples are padded by $M - N$ zeros). The modulus of the M-point DFTs are further processed so that the resonances associated with the DFT cover a band of frequencies, including the tone frequency, in symmetric fashion. Location of the subband containing the tone is achieved by finding the maximal modulus of the first $(M/2) + 1$ even (counting from zero) DFT points, A_{2k} say, and then,

if $2k \neq 0, M/2$, comparing A_{2k-1} and A_{2k+1}. The technique is exemplified in Figs. 10a and b for $M = 8$ and $N = 4$.

In the FTLS the above procedure (at stage 1) partitions the initial band $(0, f_s/2)$ to $M/2$ subbands, each of width $(f_s/2)/(M/2)$, and the tone lies unambiguously within one of the $M/2$ subbands because of oversampling. Once a tone has been located within the confines of a subband, sampling rate reduction or decimation by a factor of $M/2$ is effected. Although the tone is now undersampled, judicious choice of sampling rate reduction ratio and subband width precludes additional spectral lines from appearing within the subband containing the tone. At the reduced sampling rate again (as before), N samples of the complex tone are processed by an M-point DFT. The moduli of the M-point DFT are further processed to again achieve a symmetrical placement of the DFT's resonances across the subband of width $(f_s/2)/(M/2)$ containing the tone. Now, if in the previous stage the tone has been located in an even subband (starting with the zeroth cell), find the maximal value of $\{A_0, A_2, \ldots, A_{M/2}\}$; otherwise, find the maximal value of $\{A_{M/2}, A_{M/2+2}, \ldots, A_{M-2}, A_0\}$, say A_{2k}, and compare

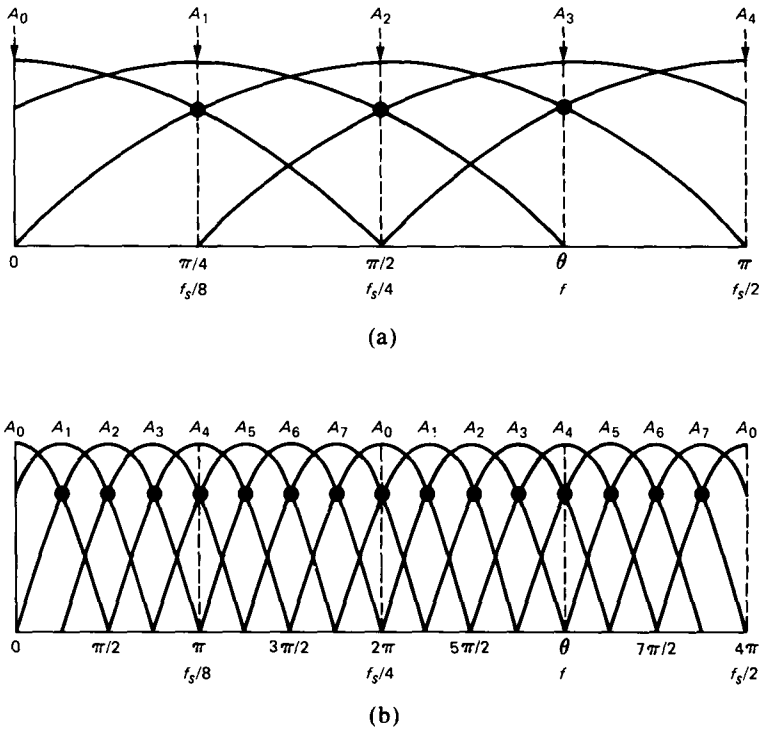

Fig. 10—Operation of the FTLS for M-8, N-4: (a) first stage, and (b) second stage.

A_{2k-1} with A_{2k+1} (provided that $k \neq 0, M/2$, for both cases). Now (after stage 2) the tone is located in a subband of width $(f_s/2)/(M/2)^2$. This process may be repeated until, finally, at the last stage, say S, the frequency subbands utilized for resolving the tone are each of width $(f_s/2)/(M/2)^S$. Note that at each stage only the even DFT coefficients and two odd DFT coefficients are needed. Moreover, a minor modification to the FTLS enables the system to test for a tone in the other band, i.e., $(f_s/2, f_s)$, provided the FTLS knows in which of the two subbands the single tone is present. Also, for $N = 2, 3$ and $M = 4$ we have a FTLS that resembles the CTLS, except for the sampling rate, which is now halved.

It should be noted that the relation $M > N$ is mandatory, and ensures that comparisons between the pertinent A_i's will be within their main lobes. Note that the ideas to combat noise presented in Section III for the CTLS pertain as well to the FTLS.

Now the FTLS is exemplified by choosing $M = 8$ and $N = 4$. Referring to Fig. 10, A_0 through A_7 are obtained from four samples of the complex tone [see (30)]. Dividing the band 0 to π into four subbands is carried out as follows:

1. The maximal value of $\{A_0, A_2, A_4\}$ is computed. From the result we decide in which of the three subbands $(0, \pi/4)$, $[\pi/4, (3\pi)/4]$, $[(3\pi)/4, \pi]$ the tone is present. If the tone is not in the subband $[\pi/4, (3\pi)/4]$, we continue to the next stage (Fig. 10b); otherwise we

2. Compare A_1 and A_3, and accordingly find in which of the two subbands, $(\pi/4, \pi/2)$ or $[\pi/2, (3\pi)/4]$, comprising the subband $[\pi/4, (3\pi)/4]$ the tone is present. Now Fig. 10b depicts how each of the four subbands in the range 0 to π of Fig. 10a may be further partitioned to isolate the tone of interest. Basically the subbands are subdivided into second-stage subbands by reducing the sampling rate by a factor of $M/2 = 4$. Now if the tone is present in an even (counting from 0) subband, $(0, \pi/4)$ or $[\pi/2, (3\pi)/4]$, find the maximal value of $\{A_0, A_2, A_4\}$. Otherwise (i.e., the tone is present in one of the odd subbands $(\pi/4, \pi/2)$ or $[(3\pi)/4, \pi]$), find the maximal value of $\{A_4, A_6, A_0\}$. If the even or odd subband output amplitude A_0 or A_4 is maximal, then continue to stage 3. If the maximal value is A_2 (even case) or A_6 (odd case), then compare A_1 with A_3 or A_5 with A_7, respectively. Now the tone has been located within a subband of width $(f_s/2)/(8/2)^2 = f_s/32$, and the processing continues in this manner until the desired frequency resolution is achieved.

V. CONCLUSION

We have presented two methods of tone location (CTLS and FTLS) as an alternative to conventional DFT. For a given requirement of N_C frequency resolution cells, a conventional DFT, which is a maximum-

likelihood estimator, uses a single transform of size N_C requiring $(N_C/2)\log_2(N_C)$ multiplications, which are the main computational burden. The associated complexity of such multiplication is eliminated in the CTLS, using a decimation scheme involving filters that have coefficients ± 1, $\pm j$, i.e., multiplier-less digital filters. For the same number of resolution cells, computational complexity is significantly reduced, at the expense of increased frequency uncertainty as a function of increasing noise. This uncertainty is decreased in the FTLS, where the cyclotomic filters of the CTLS are replaced with small DFTs (which can be repeated several times at each decimation stage). While this improved performance is at the expense of increased computational complexity (compared to the CTLS), and the resulting system does not have the optimal performance of a single DFT, the FTLS can nonetheless be preferable over a single DFT when the size of the latter makes it impractical to implement. To obtain N_C frequency resolution cells by using the FTLS in S stages, one M-point DFT is sufficient at each stage, and we have the relationship $N_C = (M/2)^S$. Hence, using the FTLS, $M = 2\sqrt[S]{N_C}$, and $S(M/2)\log_2(M)$ multiplications are sufficient for locating the tone. For example, suppose $N_C = 4096$ and $S = 4$; then $M = 16$, and the conventional DFT requires 24,576 multiplications, whereas the FTLS requires only 128 multiplications.

It follows from the simulations of the CTLS that the soft-decision method should be preferred and the filters should be operated for $N = 6$ samples. For input signal-to-noise ratios in excess of 10 dB the output signal-to-noise ratios differ from the maximal output signal-to-noise ratio by less than 0.3 dB. Finally, note that tone presence can be determined by comparing the filter outputs in the first stage to an appropriate threshold value (see Refs. 11 and 15 and the references therein).

REFERENCES

1. V. Cappelini, "Digital Filtering With Sampled Signal Spectrum Frequency Shift," Proc. IEEE, *57* (February 1969), pp. 241–2.
2. V. Cappelini, R. L. Emiliani, and A. Gabbanini, "A Special Purpose On-Line Processor for Bandpass Analysis," IEEE Trans. Audio Electroacoust., *AU-18* (June 1970), pp. 188–94.
3. J. M. Wozencraft and I. M. Jacobs, "Principles of Communication Engineering," New York: Wiley, 1967, pp. 642–5.
4. B. Gopinath and R. P. Kurshan, "A Touch-Tone Receiver-Generator With Digital Channel Filters," B.S.T.J., *55* (April 1976), pp. 455–67.
5. D. Hertz, R. P. Kurshan, and D. Malah, "Multiple Tone Detector and Locator," U.S. Patent 4,361,875, issued November 30, 1982.
6. R. P. Kurshan and D. Malah, "Broadband Cyclotomic Tone Detector," U.S. Patent 4,333,156, issued June 1, 1982.
7. D. Hertz, R. P. Kurshan, and D. Malah, "Cyclotomic Tone Detector and Locator," U.S. Patent 4,348,735, issued September 1982.
8. D. Hertz, "Digital Cyclotomic Filters and Their Applications to Signal Processing," M.Sc. Thesis, Technion-Israel Institute of Technology, June 1979.

9. D. C. Rife and R. R. Boorstyn, "Single-Tone Parameter Estimation From Discrete-Time Observations," IEEE Trans. Inform. Theory, *IT-20* (September 1974), pp. 591–8.
10. L. C. Palmer, "Coarse Frequency Estimation Using the DFT," IEEE Trans. Inform. Theory, *IT-20* (January 1974), pp. 104–9.
11. R. P. Kurshan and B. Gopinath, "Digital Single Tone Generator-Detectors," B.S.T.J., *55* (April 1976), pp. 469–96.
12. M. Onoe, "Fast Amplitude Approximation Yielding Either Exact Mean or Minimum Deviation for Quadrature Pairs," Proc. IEEE, *60* (July 1972), pp. 921–2.
13. A. Filip, "Linear Approximation to $\sqrt{x^2 + y^2}$ Having Equiripple Error Characteristics," IEEE Trans. Audio Electroacoust., *AU-21* (December 1973), pp. 554–6.
14. D. F. Freeman, "Equal Ripple Approximation for Envelope Detection," IEEE Trans. Acoust., Speech, and Signal Processing, *ASSP-26*, No. 3 (June 1978), pp. 254–6.
15. J. G. Gander, "A Pattern Recognition Approach to Tone Detection," Signal Processing, *1*, No. 1 (January 1979), pp. 65–81.

AUTHORS

David Hertz, B.Sc. and M.Sc. (Electrical Engineering), Technion-Israel Insitute of Technology, Haifa, in 1975 and 1979, respectively. He is now completing his work towards the Ph.D. degree in electrical engineering at Technion. He holds two patents with coauthors and his research interests are in digital signal processing and control theory.

Robert P. Kurshan, Ph.D. (Mathematics), 1968, University of Washington; Krantzberg Chair for Visiting Scientists, Technion, Haifa, Israel, 1976–1977; AT&T Bell Laboratories, 1968—. Mr. Kurshan is a member of the Mathematics Research Center. His current interests include formal development, specification, and analysis of distributed systems such as communication protocols.

David Malah, B.S. and M.S. (Electrical Engineering), Technion-Israel Institute of Technology, in 1964 and 1967, respectively; Ph.D. (Electrical Engineering), 1971, University of Minnesota; University of New Brunswick, Canada N.B., 1970–72; sabbatical leave, Bell Laboratories, 1979–81; Technion-Israel Institute of Technology, 1972—. At Technion-Israel Institute of Technology, he is Associate Professor of Electrical Engineering. From 1975 to 1979, and since 1981, Mr. Malah has been in charge of the Signal Processing Laboratory at Technion-Israel and is involved in research on speech and image communications, and digital signal processing techniques.

John T. Peoples, B.S.E.E., 1963, University of Detroit, M.S.E.E., 1965, and Ph.D. (Electrical Engineering), 1971, New York University; J.D., 1981, Seton Hall Law School; AT&T Bell Laboratories, 1963–1983. Present affiliation Bell Communications Research, Inc. Mr. Peoples has worked on circuit analysis and synthesis algorithms, modulation techniques, and digital signal processing methods. He is presently Attorney, Intellectual Property Matters. He holds seven U.S. patents. Senior Member, IEEE; member, Tau Beta Pi, Eta Kappa Nu. Admitted before the U.S. Supreme Court; Court of Appeals for the Federal Circuit; New Jersey Federal District Court; and New Jersey Supreme Court. Registered patent attorney in the U.S. and Canada. Member, American Bar Association; American Intellectual Property Law Association; New Jersey Bar Association; and New Jersey Patent Law Association.